From FWI to ultra-high-resolution imaging

Isabel Espin[1], Nicolas Salaun[1], Hao Jiang[1], and Mathieu Reinier[1]

https://doi.org/10.1190/tle42010016.1

Abstract

In recent years, the development of time-lag full-waveform inversion (FWI) has enabled the use of the full wavefield (primary reflections, diving waves, and their multiples and ghosts) in the inversion process. With this advancement, it is possible to obtain a very detailed velocity model, ultimately reaching the point of deriving from the velocity a migration-like reflectivity image called the FWI image. When the FWI maximum frequency is increased, high-resolution velocity models are obtained, revealing superior reservoir information compared to conventional imaging results. Two case studies will be discussed in this paper. The first is in the Greater Castberg area where the 150 Hz FWI image greatly surpassed the *Q* Kirchhoff prestack depth migration image from the water-bottom level down to the reservoir (located at a depth of about 1.5 km). The second case study is over the Nordkapp Basin. The use of the full wavefield for the shallow ultra-high-resolution (UHR) FWI image (run at 200 Hz) revealed reverse faulting and pockmark details that were invisible with Kirchhoff prestack depth migration and reverse time migration. By using additional information present in multiples, ghosts, and diving waves, a spatial resolution down to 3 m was achieved. This made it possible to image very thin features without the need for a dedicated high-resolution acquisition design. The current UHR FWI image workflow provides velocity and reflectivity information in the near surface that is important in identifying optimal locations for various purposes such as well placement and wind-turbine installation.

Introduction

New marine seismic acquisition geometries have emerged in the last few years that are designed to increase the resolution of the subsurface image. In the Barents Sea, where a strong water bottom and fast shallow sediment layers pose considerable challenges for high-resolution shallow imaging and multiple attenuation, efforts have been made to reduce the minimum recorded offset. This has been achieved by towing streamers closer to wide-towed sources (Long, 2017) or by shooting directly on top of the streamers using source-over-spread technology developed by CGG in collaboration with Lundin Energy Norway (Lie et al., 2018). To further increase the resolution, denser sampling of the subsurface has been proposed where the cable and receiver separation is reduced and the sources and streamers are kept at a shallow depth to avoid ghost interference (Garden et al., 2017).

While these new acquisition designs have greatly improved the imaging resolution (Salaun et al., 2019), when imaged with conventional processing, only primary reflection waves are considered. Other types of waves such as multiples, ghosts, and transmitted waves are treated as noise. With recent advancements in compute power and inversion algorithms, full-waveform inversion (FWI) is now able to reach the maximum frequency bandwidth of the seismic data (Kalinicheva et al., 2021). By adding more resolution in the velocity field, rapid velocity changes can be captured, improving the quality and authenticity of the migration image (Salaun et al., 2022). In addition to enhancing the migration image, access to a high-resolution velocity field provides useful information about the nature of the imaged subsurface (Lu, 2016; Shen et al., 2018; Salaun et al., 2021; Tang et al., 2021). To visualize the velocity field in a way that is consistent with conventional migration images, Zhang et al. (2020) propose a time-lag FWI (TLFWI) workflow to directly output the reflectivity image. They refer to this as FWI imaging and the resulting reflectivity as the FWI image. FWI imaging uses the full-wavefield data including primaries, diving waves, and their multiples and ghosts. It provides an elegant solution to obtain a reflectivity image without performing the usual preprocessing and migration steps. An additional advantage of FWI imaging is being able to directly use raw recorded seismic data. This avoids possible data damage during the denoise, deghost, and demultiple stages. By its very nature, FWI imaging uses the full wavefield and least-squares data fitting. Thus, it can extract the full benefit of seismic data for optimal low- and high-wavenumber resolution with superior signal-to-noise ratio (S/N) and focusing. This method has proven to be very efficient in the case of a complex velocity field such as a large salt body or gas cloud (Huang et al., 2021). In addition, Wei et al. (2021) demonstrate that FWI imaging with a frequency (100 Hz or higher) close to the limit of temporal resolution of seismic data can provide seismic images of unprecedented resolution. This is impossible to achieve with conventional imaging methods.

By combining FWI imaging with the source-over-spread acquisition design (Vinje et al., 2017), we present two case studies in which FWI imaging outperforms conventional imaging methods (Kirchhoff prestack depth migration [KPSDM] and reverse time migration [RTM]) in terms of image resolution. For both cases, the data were acquired with the source-over-spread design that deploys wide-towed sources on top of the streamer spread in combination with a large front source (Vinje and Elbouth, 2019). The first case is from the Greater Castberg area and aims to image a reservoir over complex fault blocks. The second case concerns the Nordkapp Basin, where the imaging target is the Carnian Sand packages next to large salt bodies (Dhelie et al., 2021). In the following sections, we highlight the multiple benefits of enhanced resolution for reservoir definition, drilling derisking, and better geologic understanding of the top of salt.

From high-resolution velocity to reflectivity over the Greater Castberg area

The Greater Castberg survey is located in the northeast of the Barents Sea and covers an area of 5200 km^2. The main hydrocarbon

[1]CGG, Massy, France. E-mail: isabel.espin@cgg.com; nicolas.salaun@cgg.com; hao.jiang@cgg.com; mathieu.reinier@cgg.com.

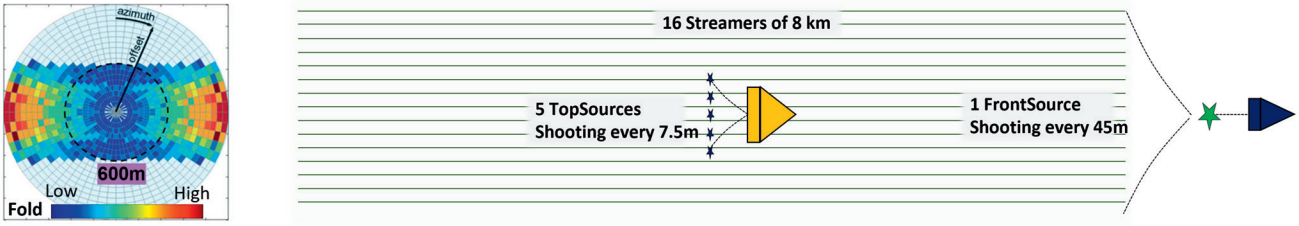

Figure 1. Acquisition design used to acquire the Greater Castberg area, Barents Sea. This design was optimized for cost-effective acquisition, limiting the number of sailed lines needed to cover the 5200 km^2 survey.

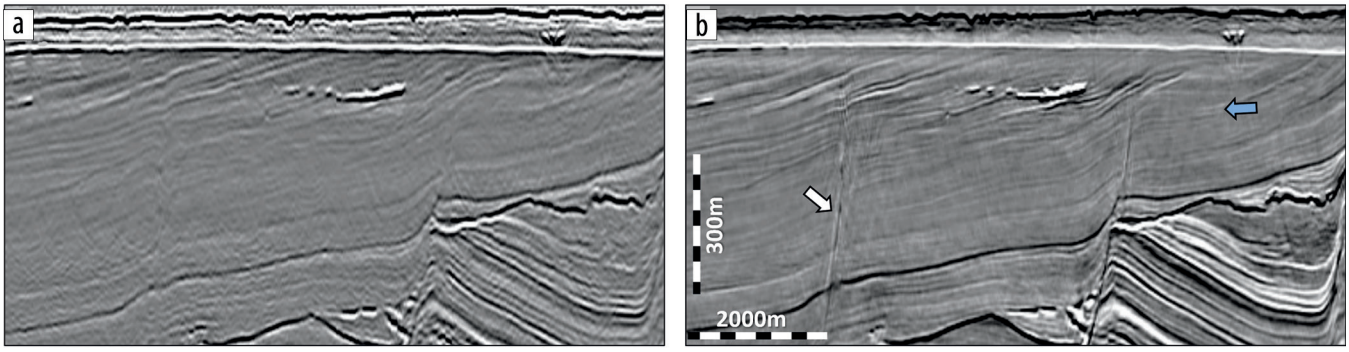

Figure 2. Impact of the source-over-spread design. (a) The legacy image from a conventional towed-streamer acquisition, with minimum recorded offset of 200 m. (b) The KPSDM image obtained with the source-over-spread design benefiting from the full near-offset coverage. Both faulting (white arrow) and thin sediment layers (blue arrow) are revealed with the source-over-spread design.

discoveries in the area have been made in the Early to Middle Jurassic formations and within the Early Cretaceous formations. These discoveries are often located on rotated fault blocks where gas and oil were proven in sandstone reservoirs. With the objective to (1) image the fault network with high resolution and (2) reveal untested leads that may bring additional prospects to Johan Castberg Field in the future, the survey was acquired with a source-over-spread design in 2019. This design comprised a front source and a top source, towed at depths of 7.5 and 5 m, respectively. The top source fired on top of an array of 16 streamers that were 8 km long and towed at a variable depth of approximately 5 to 50 m. While the sources on top of the streamers aim to record full-azimuth near-offset data for high-resolution shallow imaging and improved multiple attenuation, the source at the front of the streamer spread aims to record long offsets for FWI purposes (Figure 1). The diving-wave penetration depth is doubled due to this front source, reaching a depth of about 2 km. This is the depth at which most known reservoirs are located, right below the base Cenozoic unconformity. With a natural bin size of 6.25 × 6.25 m, the final KPSDM obtained from these data showed a great uplift compared to the legacy volume, especially in terms of lateral resolution and fault imaging (Figure 2). Furthermore, as a result of the dual-azimuth recording, the fold in the near-offset range is doubled. This widely increases the S/N of the near surface and reveals the presence of thin sediment layers below the water bottom (located at a depth of about 400 m) that are barely visible with conventional acquisition.

For the velocity model building, an initial model was built from joint reflection-refraction tomography (Allemand et al., 2020). This made it possible to decouple the velocity from the anisotropy by using both residual moveout and first-break information. After the anisotropy estimation step, it was possible to use the full raw recorded data without any muting in the FWI process. Cycle skipping and amplitude discrepancy occurring between modeled and observed seismic data were mitigated through TLFWI, which uses a time-lag cost function (Zhang et al., 2018). Density is derived when inverting V_p with acoustic FWI based on the Gardner law. After each FWI frequency inversion, the density is updated accordingly using this law based on the updated V_p model. For the initial part of the velocity model building, the wavelet was extracted from near-field hydrophone (NFH) recordings. Later in the flow, wavelets are inversion based and extracted from the full record length and limited to 1.5 km offsets. Over the 400 km^2 Johan Castberg Field, TLFWI was initially run up to 60 Hz (Figure 3). At such a frequency, the velocity field accurately follows the geologic layers, delineating both the thick lithological layers and the thin sediment bands. The resulting detailed velocity demonstrated its value because it also captured reservoir features such as fluid contacts and strong flat-spot signatures. The rich low wavenumbers in the velocity model allow for clear delineation of the reservoir and hydrocarbon presence. Additional details can be seen through clear vertical compartmentalization of multiple flat spots. When the FWI frequency is increased to 90 Hz over a targeted reservoir area, thinner details are revealed, possibly related to the change in the type of fluids present in the sand packages. The increased lateral resolution also made it possible to delineate the reservoirs, providing useful information about their potential volume content. This velocity field could then be used as an additional attribute to better characterize known and unknown prospects.

While some high-wavenumber velocity features may not change the kinematics of the migrated image, these additional details can be of great value for FWI images. In the Greater Castberg project, where the processing was performed with a 2 ms sampling rate,

DOI:10.1190/tle42010016.1

the expected resolution of the final full-stack KPSDM was close to 150 Hz with a good S/N level. The FWI image was then increased to a similar frequency to compare with KPSDM in order to appreciate the benefits of using the full wavefield with full bandwidth in addition to the least-squares nature of the FWI process. While the vertical resolution of the FWI image is comparable to the vertical resolution of the conventional image (3 m), the lateral resolution of the FWI image (3 m) is much improved compared to the KPSDM image. This is due to the near-offset primaries being well recorded during this survey and because FWI takes advantage of the diving-wave and multiple energy, as well as the ghost information associated with a cable depth of 30 m.

Figure 4 shows a comparison of the KPSDM image using an advanced preprocessing flow and the 150 Hz FWI image using raw recorded shot gathers. In this cross section, the geology is relatively simple. It does not show strong velocity contrasts or complex wavepaths. Nevertheless, the benefits of FWI imaging can be clearly seen. The FWI image shows a considerable uplift in terms of lateral resolution, revealing thin faulting and discontinuities in the main seismic events; whereas, the sharp pseudovertical or reversed faults are aliased on the KPSDM image, even with a small natural bin size of 6.25 m. They are well represented on the FWI image. On this image, geologic features with a thickness of less than 10 m can be identified, even at a recorded depth of 1 km (a depth at which strong multiple curtains are observed on the raw data). To handle the complex multiple generation in the forward modeling, it is key to fully recover the true contrast at the water-bottom level. Therefore, no constraints are set in the water layer, allowing the FWI to change the water-column velocity and water-bottom depth to accurately update this contrast. As frequency and iterations increase, the contrast becomes increasingly accurate, making it

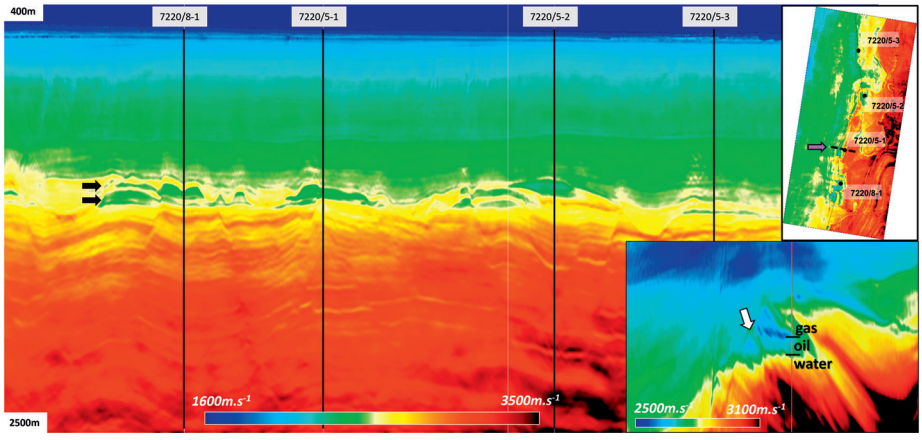

Figure 3. FWI velocity extracted from a random line crossing various Johan Castberg reservoirs. Details in the velocity field make it possible to observe geologic layering and detect superimposed reservoirs (black arrows) over this 400 km^2 area. In the right part of the figure, velocity at 90 Hz in a subline crossing well 722/5-1 (violet arrow shows subline location) obtained from FWI is displayed. A clear separation between the three different fluid phases can be observed, with the gas at the top in dark blue, followed by the oil and water in green. In addition to this fluid type, the displayed velocity clearly shows the lack of continuity between the two reservoirs (white arrow).

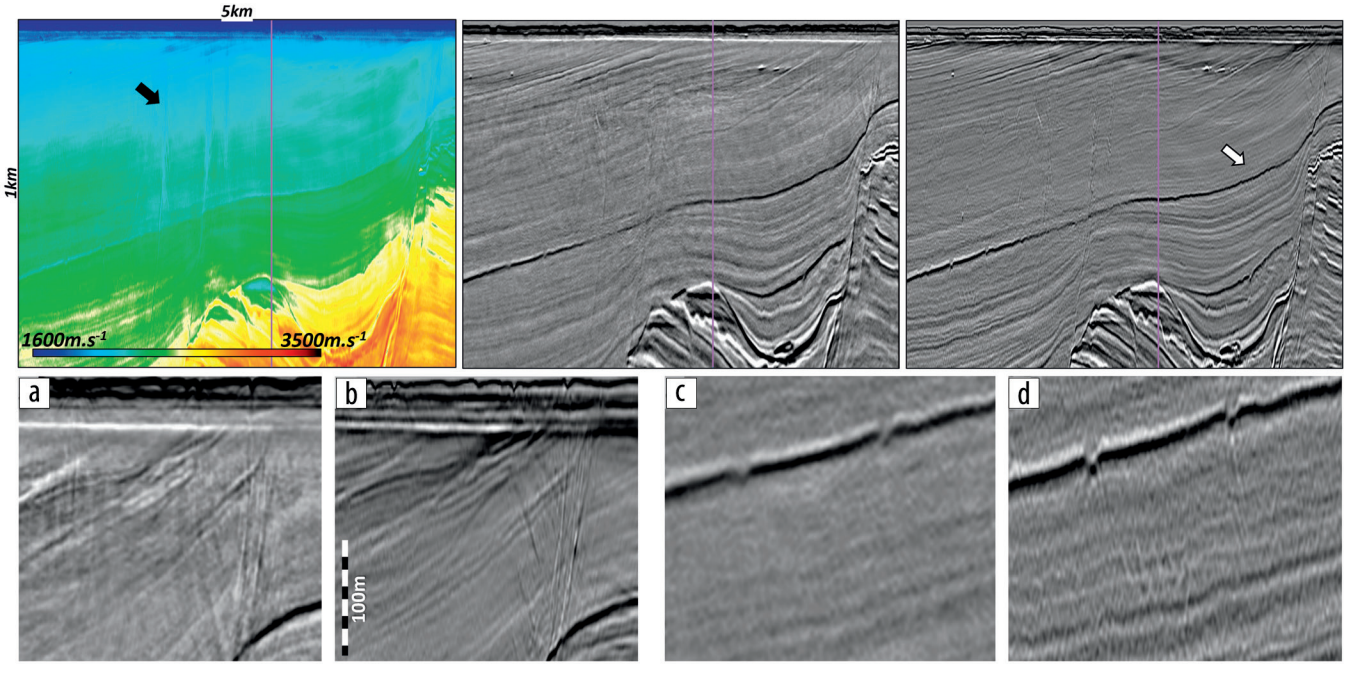

Figure 4. The top panels show the FWI velocity obtained at 150 Hz (left) with the well location indicated by the purple line, the final KPSDM image (center), and the FWI image (right) at 150 Hz. Large sharp faulting is more visible on the FWI image and can also be observed on the velocity. This is highlighted by a low-velocity trend, indicating the presence of gas leaking toward the surface (black arrow). The base Cenozoic (white arrow) appears more discontinuous and affected by the underlying faulting system. On the (a) KPSDM and (b) FWI image close-ups, shallow faults and their reversed dip parts can be clearly interpreted on the FWI image while tending to be blurry on the conventional image. Moreover, the (d) very thin faulting system present below the base Cenozoic is revealed on the FWI image (c) while looking smoothed on the KPSDM.

DOI:10.1190/tle42010016.1

DOI:10.1190/tle42010016.1

possible to fully model the water-layer-related reflections (multiples and ghosts) and ensuring their full use to recover the subsurface velocity and reflectivity.

In the Johan Castberg area, FWI imaging brings additional resolution to gain a better understanding of the sharp faulting and the possible segmentation of the reservoir. Figure 5 compares a conventional image and an FWI image in terms of focusing at the reservoir level for both the cross section and depth slice. On the cross section, with the improvement in vertical resolution mainly due to the increased near-angle illumination from multiple energy (Wei et al., 2021), it is possible to separate thin sand layers and gain a better understanding of the sediment deposits present either above or below the reservoir as well as the faulting systems. On the depth slice, with the improved lateral resolution, it is possible to detect faulting in the reservoir, indicating possible segmentation. In these proposed examples, using FWI from raw data has the ability to outperform high-end processing and imaging. By not having to perform the complex denoising and wavefield separation steps needed to isolate primary reflected energy, this has not only greatly simplified the imaging sequence but also completely retained all of the useful energy in the input data.

FWI imaging for UHR in the Nordkapp Basin

The second case study in this paper discusses the use of FWI imaging in the Nordkapp Basin to image the shallow subsurface with UHR. This 3700 km^2 basin, also located in the Barents Sea, is an underexplored salt basin with expected hydrocarbon traps located at depths of approximately 3 km. Similar to the previous case study, a source-over-spread acquisition design was selected to achieve high-resolution imaging of the stratigraphic traps. Acquisition consisted of a hexasource towed at a depth of 5 m and 18 cables towed at a depth of 30 m and with a separation of 75 m. This design was combined with sparse nodes to better illuminate the deep salt flanks (Lie et al., 2022). In addition to imaging the deep target, a high-resolution image of the shallow subsurface was performed to assess potential shallow drilling hazards. Imaging the near surface with high resolution is possible with this design due to the full-azimuth coverage achieved from zero angle up to the critical incidence angle at approximately 900 m offset and up to 1 km in depth. Moreover, this full-azimuth coverage guarantees a high S/N and ample illumination of the shallow subsurface. Here, we describe in detail various applications of TLFWI to achieve (1) shallow high-resolution imaging to derisk drilling, (2) FWI image angle gathers to extend the use of FWI imaging to quantitative interpretation, and (3) detailed velocity fields to improve top-of-salt imaging and salt-mechanism understanding.

Compared to conventional UHR acquisition designs, the source-over-spread acquisition design has a much sparser receiver grid sampling, with a surface sampling of 12.5 m in the *x* direction and 75 m in the *y* direction along and perpendicular to the shooting direction, respectively. Initially, high-resolution RTM was performed to provide a shallow image in order to derisk drilling in cases of shallow gas accumulations, shallow faulting, and iceberg scours. Here, we compare the impact of different processing methods such as interpolation, multiple imaging, and FWI imaging. Figure 6 shows the results from these different imaging technologies for the first 80 m of the subsurface between the water bottom and the base Quaternary.

The data interpolation flow applied on the input data prior to migration aimed to reduce the *y* sampling of the primary reflections down to 12.5 m (equal to the *x* sampling). We tested both a simple 2D interpolation and an advanced 5D interpolation (Poole, 2010). We then compared the two approaches (Figures 6a and 6b). While the 2D interpolation has difficulty in recreating the data using only one spatial and one temporal dimension, the 5D interpolation performs a mapping from natural grid to optimal grid. This results in a denser acquisition using more dimensions and incorporating information from different shot points and shot lines. While iceberg scour aliasing is well mitigated with 5D interpolation, the illumination provided by the primary reflections is limited. The next step is to use the information present in the multiples through multiple imaging (Figure 6c). This technique, based on least-squares one-way wave-equation migration (Poole, 2021), uses the various orders of the recorded multiples, which contain richer subsurface illumination information and smaller reflection angles than primary reflection energy. Its uses make it possible to efficiently reduce aliasing and acquisition imprint, easing iceberg scour delineation.

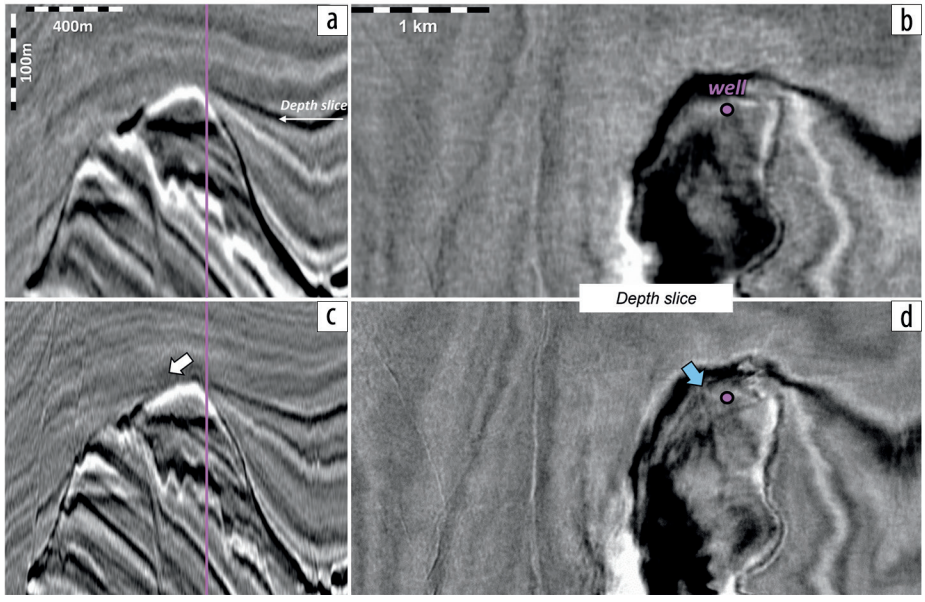

Figure 5. (a) KPSDM and (c) FWI imaging sections crossing the reservoir, visible with its flat spot. (c) On the FWI image, thin sediment layers with a mild impedance contrast are visible above the reservoir (white arrow). With the increased near-angle illumination from multiple energy, the FWI image shows a higher vertical resolution that is better at defining the geologic events. On the depth slices, the lateral resolution visible in (d) the FWI image sharpens the main faults and reveals thin faulting inside the reservoir compared to (b) KPSDM.

Finally, FWI imaging (Figure 6d) can infill illumination gaps in primary reflections by inverting the multiple, ghost, and transmitted energy. Therefore, the use of the full wavefield overcomes the aliasing and acquisition footprint problems. The additional illumination provided by FWI imaging enables a better understanding of geologic features such as iceberg scours and shallow gas pockets. The continuity of the iceberg scours (visible at 300 m depth) is much improved, and even thinner scours are revealed that were not visible with conventional imaging. The shallow gas pockets are better delineated, and the heterogeneities within the bodies are clearer.

High-resolution imaging was performed over potential hydrocarbon accumulations to identify shallow hazards prior to drilling. When increased to 200 Hz, FWI imaging can theoretically attain

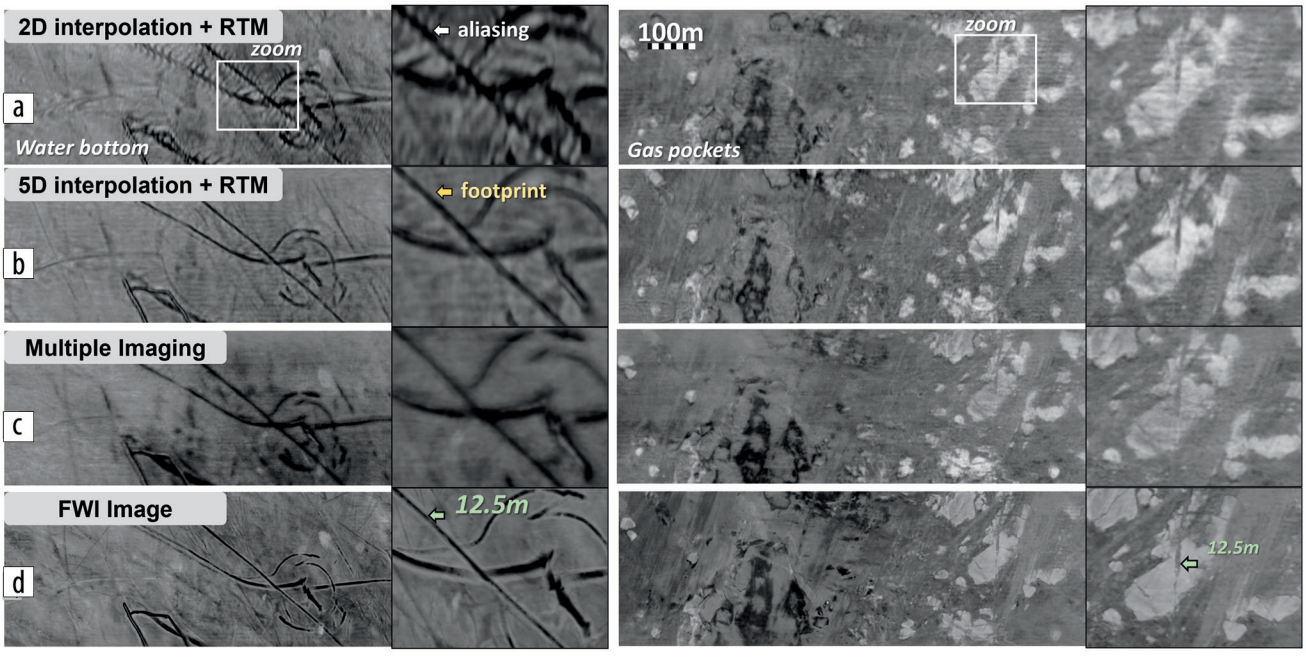

Figure 6. Overcoming coarse cable sampling. An imaging test at depths of 300 m (left) and 380 m (right) shows iceberg scours and shallow gas pockets, respectively. The different imaging methods used were (a) 2D interpolation and (b) 5D interpolation, followed by a 200 Hz RTM migration, (c) multiple imaging, and (d) FWI imaging.

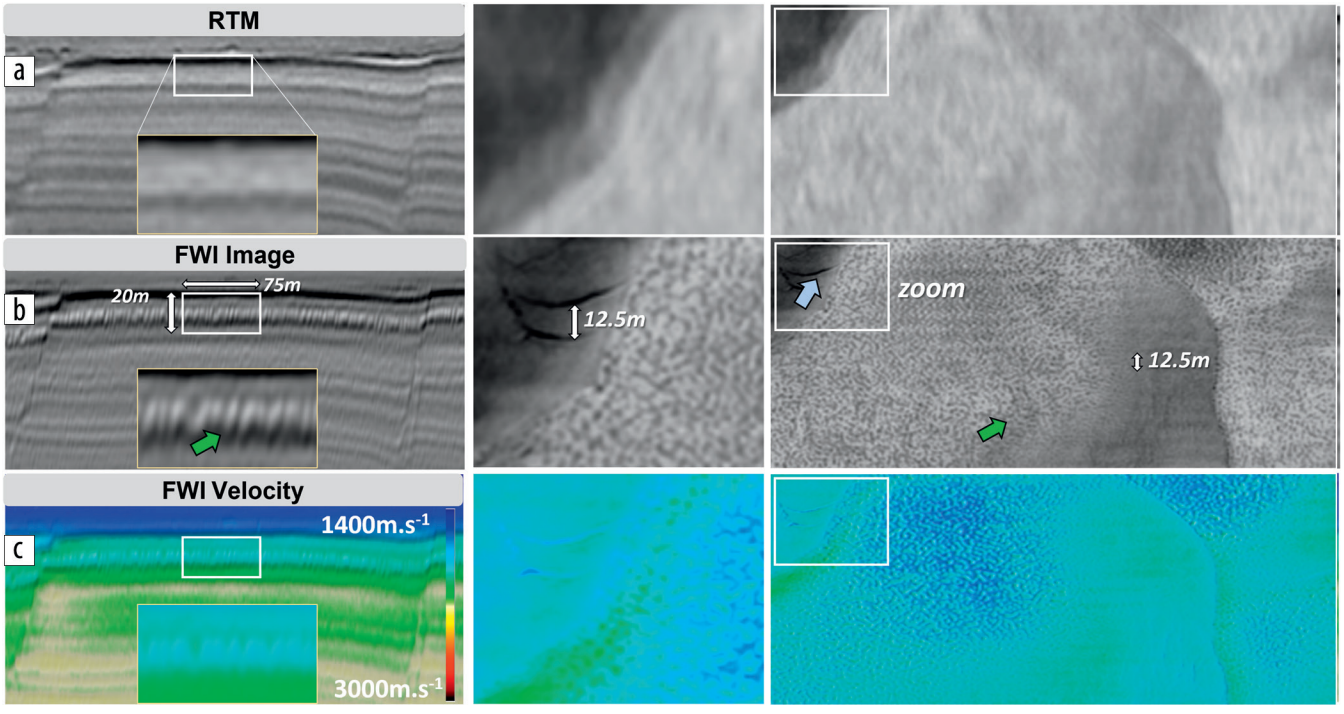

Figure 7. Pockmark imaging. From top to bottom, comparison between (a) 200 Hz RTM image, (b) the FWI image, and (c) the FWI velocity model. From left to right are section view, depth slice at 400 m of depth, 20 m below the water bottom, and a zoom of the depth slices shown. With FWI image resolution, it is possible to image pockmarks as small as 8 m wide (green arrows) as well as sharp faulting (blue arrows).

DOI:10.1190/tle42010016.1

a maximum resolution of less than 4 m, providing a UHR image of the shallow subsurface. If we compare Figures 7a and 7b, the superior lateral resolution achieved with FWI imaging compared to RTM makes it much easier to identify thin pockmark features (only 8 m wide) 20 m below the water bottom in both the depth slice and section view. Pockmarks can be considered a geohazard because they often indicate the presence of shallow gas or overpressured pore fluids. This is particularly important when analyzing the sediment composition and consolidation for wind farms (Velenturf et al., 2021). This underlines the potential of the technique not only for preventing drilling hazards but also for wind-turbine foundation planning.

Performing FWI makes it possible to obtain both the reflectivity of the subsurface and the velocity information (Figure 7c). This detailed velocity field provides an indication of the velocity variations of the rock properties in the near surface, such as a slower velocity package within the pockmarks, indicating potential unconsolidated material. This information is crucial for the oil and gas industry and is also valuable for wind-farm installation planning (Karkov et al., 2022).

In this salt basin context, FWI imaging was also performed to map the top of salt and better understand the mechanisms that controlled the salt movement. The selected area covers a massive salt body, reaching the water-bottom surface at a depth of 280 m and extending approximately 7.5 km wide and up to 8 km long. Figure 8a shows a depth slice of the 200 Hz FWI velocity model, crossing the top of salt at a depth of approximately 400 m. The lateral heterogeneity of this top of salt is visible, with velocities varying from 2500 to 6500 m/s^{-1}. A hypothesis about the origin of these heterogeneities can be suggested, such as the presence of Upper Paleozoic carbonates (Rafaelsen et al., 2003) and/or a cap-rock formation associated with episodes of exposure of these evaporites to the surface (Stadtler et al., 2014). Figures 8b and 8c show a section of the FWI velocity model and FWI image, respectively, highlighting the presence of carbonate packages above the homogeneous halite body. Deeper within the salt diapir, intrasalt heterogeneities are visible. This indicates the presence of evaporitic lithologies other than pure halite. The alignment of the intrasalt features (in this case, north-south) is useful to better understand the stress mechanism that generated this salt movement and identify possible diapir shear zones. To identify the top of the halite salt, access to high-resolution FWI velocity in addition to the FWI image is crucial. The sharp contrast of halite velocity (4500 m/s^{-1}) is clearly visible on the velocity field and not obvious on the FWI image (Figure 8c). In Figure 8d, when the top of salt is imaged with conventional KPSDM using a 10 Hz FWI model, events can be misplaced, and the top of salt is distorted. On the contrary, in the FWI image, the top-of-salt heterogeneities are clearer. This, combined with the information from the velocity model, offers a better geologic understanding of the complex top of salt. In addition to providing useful information to understand basin evolution, industry interest in understanding these bodies has increased due to their potential for gas and hydrogen storage in salt caverns. For these reasons, delineating the salt geometry, mapping intrasalt heterogeneities, identifying intradiapir shear zones, and studying the top of salt are critical for planning and derisking salt caverns and associated drilling.

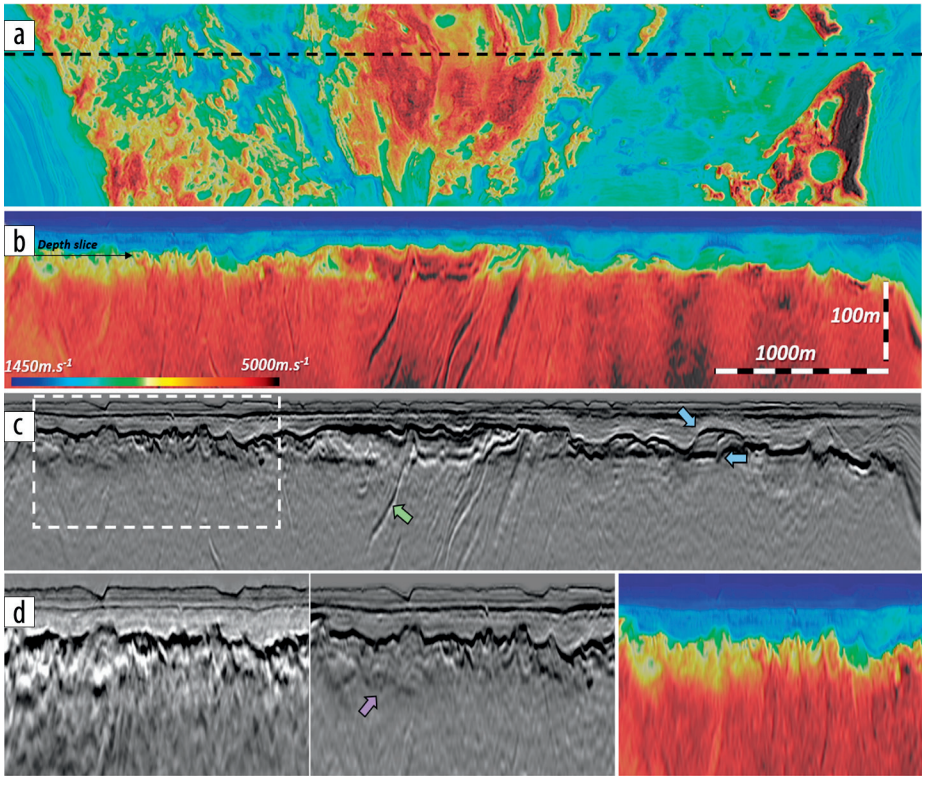

Figure 8. Comparison of the 200 Hz FWI image, FWI velocity, and KPSDM image to study the top-of-salt and intrasalt heterogeneities. (a) FWI velocity model at a depth of 400 m showing strong lateral variations in velocity at the top of salt. (b) FWI velocity and (c) FWI image in section view showing fast velocity features, suggesting contorted anhydrite layers inside the salt (green arrow) and carbonate packages (blue arrows). (d) When comparing KPSDM, FWI image, and FWI model, FWI image reveals complex faulting structure (violet arrow) present above the salt body that is invisible in KPSDM.

Impact of acquisition design

The two case studies presented in this paper are based on the source-over-spread acquisition design and FWI imaging. To assess the impact of this solution and the feasibility of using different acquisition designs for UHR studies, FWI imaging was performed using different offset limits and azimuths. Figure 9 shows the results of the three different acquisition designs used to perform FWI imaging. In the first case, the FWI image was generated with a source-over-spread design with a maximum offset of 2 km (Figure 9a). In the second case, a conventional half-spread acquisition design was simulated with a minimum offset of 200 m (Figure 9b). Finally, in the third case, the gun density was artificially divided by two and the maximum offset was

DOI:10.1190/tle42010016.1

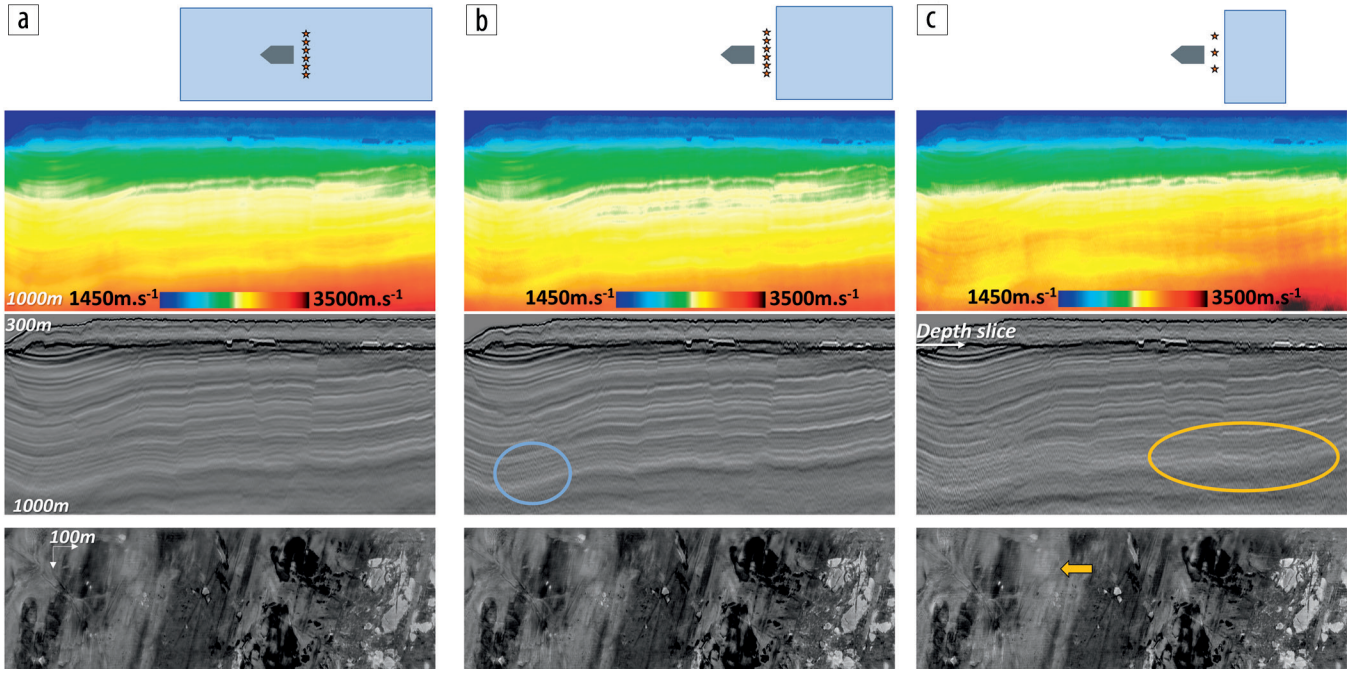

Figure 9. Impact of acquisition design in the FWI image. Three acquisition designs are compared including (a) source-over-spread acquisition with a 2 km maximum offset, (b) a conventional design with six sources and a minimum 200 m offset, and (c) a conventional design with three sources and a maximum 1 km offset. From top to bottom are the velocity model, FWI image in section view, and FWI image in depth slice at 400 m showing shallow gas pockets. When the dual-azimuth and near-offset data are removed, the FWI image appears noisier at a depth of about 800 m (blue circle). When the maximum offset is limited to 1 km, the kinematics is affected below 800 m, degrading event focusing and structure continuity (orange circle). The reduction in source number creates mild striping that is visible in the depth slice (orange arrow). Overall, for near-surface imaging purposes, design (c) appears to be sufficient.

decreased to 1 km to mimic a more affordable acquisition (Figure 9c). For all three cases, FWI was run from 4 to 100 Hz to assess the quality of the velocity and image obtained. Using case 1 as our reference, it can be observed that case 2 provides an overall similar resolution to case 1. However, a difference in S/N can be observed in the deep part of the section (below 500 m) due to the absence of the split-spread information. The absence of the very near offset does not affect the resolution of the near-surface image. In case 3, limiting the maximum offset to 1 km has a strong impact on the stability of the inverted velocity, especially below a depth of 500 m. In this case, kinematic distortion and lack of event focusing are observed. Using three guns instead of six tends to slightly increase the acquisition footprint, but the resolution of the depth slice remains of high quality. Overall, this decimation feasibility study shows that it is possible to extend FWI imaging to different acquisition designs and possibly to vintage acquisitions to obtain UHR images in the very shallow subsurface, as in this example within the first 500 m of depth. On the other hand, for deeper targets, recording longer-offset and dual-azimuth data greatly improves the kinematic update and S/N for the FWI image. The importance of the initial velocity model used for FWI imaging also becomes critical when seeking deeper imaging targets.

Conclusions

New marine acquisition designs have recently been implemented to provide the required data for advanced imaging technology to improve subsurface imaging resolution, and hence to better understand known hydrocarbon reservoirs and possibly discover new ones. The demand for UHR surveys has also increased over the last few years, notably to better characterize the near surface, avoid drilling hazards, and to plan wind-turbine foundations. In the conventional seismic imaging approach, only the reflection wavefield is utilized to form the image, and the resolution is limited by the acquisition sampling and the usable bandwidth of the recorded signal.

In this paper, we demonstrated that FWI imaging is an impactful technique that is able to considerably increase the seismic imaging resolution when the full wavefield is used in the least-squares inversion process. All recorded multiple, ghost, and diving waves, originally treated as noise in conventional imaging, can now be fully exploited to obtain high-resolution images and better characterize the shallow subsurface. FWI imaging not only delivers improved resolution of shallow heterogeneities, it also reduces their positioning uncertainty thanks to the accurate velocity model that makes it possible to locate the events at their true geologic positions. With recent advancements in elastic FWI, extraction of rock-property information from the raw data becomes possible.

On the basis of these results, it is possible to reconsider optimal UHR acquisition designs tailored specifically for advanced FWI imaging. Given current industry requirements for high-quality data for improved target imaging, the use of sparse nodes simultaneously with source-over streamer acquisition can be the ultimate acquisition design. This design, together with the benefits of advanced FWI imaging, can greatly improve imaging quality and reduce the costs and risks along the exploration and production workflow, from shallow to deep. TLE

Acknowledgments

We thank Lundin Energy, CGG Earth Data, and TGS for permission to publish this work. We also thank our colleague Daniela Donno for useful discussions.

Data and materials availability

Data associated with this research are confidential and cannot be released.

Corresponding author: isabel.espin@cgg.com

References

Allemand, T., A. Sedova, G. Lambaré, D. Grenié, and P. Guillaume, 2020, Full waveform inversion in an anisotropic earth: A practical workflow: 82nd Conference and Exhibition, EAGE, Extended Abstracts, https://doi.org/10.3997/2214-4609.202011685.

Dhelie, P. E., V. Danielsen, and J. Lie, 2021, Combining nodes and streamers to tackle the imaging challenges of salt basins in the Barents Sea: First International Meeting for Applied Geoscience & Energy, SEG/AAPG, Expanded Abstracts, 41–45, https://doi.org/10.1190/segam2021-3594693.1.

Garden, M., O. Michot, M. Terenzoni, H. Veire, J. Granli, L. Moskvil, and K. Krathus-Larsen, 2017, Resolution, resolution, resolution — An ultra-high resolution seismic case study from the Barents Sea: 79th Conference and Exhibition, EAGE, Extended Abstracts, https://doi.org/10.3997/2214-4609.201701138.

Huang, R., Z. Zhang, Z. Wu, Z. Wei, J. Mei, and P. Wang, 2021, Full-waveform inversion for full-wavefield imaging: Decades in the making: The Leading Edge, **40**, no. 5, 324–334, https://doi.org/10.1190/tle40050324.1.

Kalinicheva, T., M. Warner, and F. Mancini, 2021, Full-bandwidth FWI: 82nd Conference and Exhibition, EAGE, Extended Abstracts, https://doi.org/10.3997/2214-4609.202010246.

Karkov, K., E. Dalgaard, A. Diaz, H. Duarte, H. Hansen, S. Hviid, and N. C. H. van Gilse et al., 2022, Case study: AVO inversion and processing of ultra-high resolution seismic for a windfarm application: 83rd Conference and Exhibition, EAGE, Extended Abstracts, https://doi.org/10.3997/2214-4609.202210942.

Lie, J., V. Danielsen, P. Dhelie, R. Sablon, R. Siliqi, C. Grubb, V. Vinje, C. Nilsen, and R. Soubaras, 2018, A novel source-over-cable solution to address the Barents Sea imaging challenges: Marine Acquisition Workshop, EAGE, Extended Abstracts, https://doi.org/10.3997/2214-4609.201802101.

Lie, J.-E., V. Vetle, P. Dhelie, H. Jiang, V. Danielsen, and N. Salaun, 2022, Nordkapp topseis/node acquisition — Lessons from a modelling study: First Break, **40**, no. 2, 41–49, https://doi.org/10.3997/1365-2397.fb2022011.

Long, A., 2017, Source and streamer towing strategies for improved efficiency, spatial sampling and near offset coverage: First Break, **35**, no. 11, https://doi.org/10.3997/1365-2397.35.11.90385.

Lu, R., 2016, Revealing overburden and reservoir complexity with high-resolution FWI: 86th Annual International Meeting, SEG, Expanded Abstracts, 1242–1246, https://doi.org/10.1190/segam2016-13872562.1.

Poole, G., 2010, 5D data reconstruction using the anti-leakage Fourier transform: 72nd Conference and Exhibition, EAGE, Extended Abstracts, https://doi.org/10.3997/2214-4609.201400654.

Poole, G., 2021, Least-squares multiple imaging constrained jointly by OBN and towed-streamer data: 82nd Conference and Exhibition, EAGE, Extended Abstracts.

Rafaelsen, B., K. Andreassen, T. Samuelsberg, K. Hogstad, and T. Randen, 2003, Upper Paleozoic carbonate build-ups in the Norwegian Barents Sea — New insights from 3-D seismic and automated facies mapping: 65th Conference and Exhibition, EAGE, Extended Abstracts, https://doi.org/10.3997/2214-4609-pdb.6.E41.

Salaun, N., G. Henin, A. Wright, S. Pellerin, J. Deprey, B. Deschizeaux, V. Souvannavong, P. Dhelie, and V. Danielsen, 2019, Capturing the value of high resolution source-over-streamer acquisition at Barent Sea: 81st Conference and Exhibition, EAGE, Extended Abstracts, https://doi.org/10.3997/2214-4609.201901178.

Salaun, N., M. Reinier, I. Espin, and G. Gigou, 2021, FWI velocity and imaging: A case study in the Johan Castberg area: 82nd Annual Conference and Exhibition, EAGE, Extended Abstracts, https://doi.org/10.3997/2214-4609.202112763.

Salaun, N., A. Wright, A. Pintus, H. Jiang, L. Janot, A. Roodaki, P. Dhelie, J. Lie, and V. Danielsen, 2022, High-resolution full-waveform inversion for structural improvement and prospects delineation: A case study at Haugaland High: 83rd Annual Conference and Exhibition, EAGE, Extended Abstracts, https://doi.org/10.3997/2214-4609.202210428.

Shen, X., L. Jiang, J. Dellinger, A. Brenders, C. Kumar, M. James, J. Etgen, D. Meaux, R. Walters, and N. Abdullayev, 2018, High-resolution full-waveform inversion for structural imaging in exploration: 88th Annual International Meeting, SEG, Expanded Abstracts, 1098–1102, https://doi.org/10.1190/segam2018-2997202.1.

Stadtler, C., C. Fichler, K. Hokstad, E. Myrlund, S. Wienecke, and B. Fotland, 2014, Improved salt imaging in a basin context by high resolution potential field data: Nordkapp Basin, Barents Sea: Geophysical Prospecting, **62**, no. 3, 615–630, https://doi.org/10.1111/1365-2478.12101.

Tang, Y., D. Gaines, J. Hefti, S. Every, E. Neumann, and R. Pharis, 2021, Land full-wavefield inversion for addressing complex near-surface challenges in the Delaware Basin: First International Meeting for Applied Geoscience & Energy, SEG/AAPG, Expanded Abstracts, 702–706, https://doi.org/10.1190/segam2021-3594001.1.

Velenturf, A., A. Emery, D. Hodgson, N. Barlow, A. Mohtaj Khorasani, J. Van Alstine, E. L. Peterson, S. Piazolo, and M. Thorp, 2021, Geoscience solutions for sustainable offshore wind development: Earth Science, Systems and Society, https://doi.org/10.3389/esss.2021.10042.

Vinje, V., and T. Elboth, 2019, Hunting high and low in marine seismic acquisition; combining wide-tow top sources with front sources: 81st Conference and Exhibition, EAGE, Extended Abstracts, https://doi.org/10.3997/2214-4609.201900899.

Vinje, V., J. Lie, V. Danielsen, P. Dhelie, R. Siliqi, C. Nilsen, E. Hicks, C. Walters, and A. Camerer, 2017, Shooting over the streamer spread; a novel approach in seismic marine acquisition and imaging: 79th Conference and Exhibition, EAGE, Extended Abstracts, https://doi.org/10.3997/2214-4609.201700838.

Wei, Z., J. Mei, Z. Wu, Z. Zhang, R. Huang, and P. Wang, 2021, FWI imaging: Revealing the unprecedented resolution of seismic data: First International Meeting for Applied Geoscience & Energy, SEG/AAPG, Expanded Abstracts, 682–686, https://doi.org/10.1190/segam2021-3583772.1.

Zhang, Z., J. Mei, F. Lin, R. Huang, and P. Wang, 2018, Correcting for salt misinterpretation with full-waveform inversion: 88th Annual International Meeting, SEG, Expanded Abstracts, 1143–1147, https://doi.org/10.1190/segam2018-2997711.1.

Zhang, Z., Z. Wu, Z. Wei, J. Mei, R. Huang, and P. Wang, 2020, FWI imaging: Full-wavefield imaging through full-waveform inversion: 90th Annual International Meeting, SEG, Expanded Abstracts, 656–660, https://doi.org/10.1190/segam2020-3427858.1.